Integration of quantum dot light sources

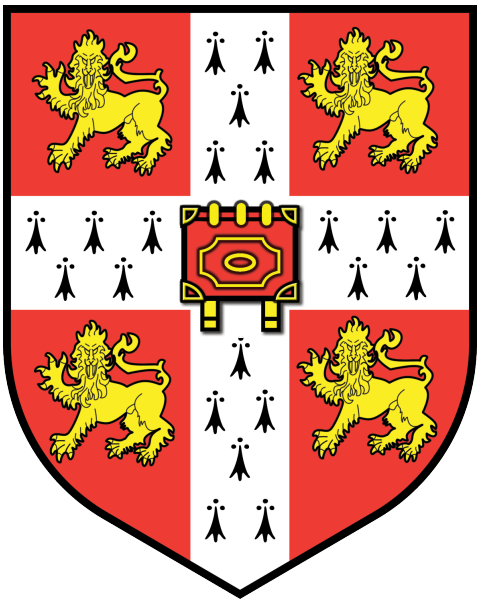

Eoin Murray

Magdalene College

Department of Physics

University of Cambridge

2015

This dissertation is submitted for the degree of

Master of Philosophy

Declaration

This dissertation is the result of my own work and includes nothing which is the outcome of work done in collaboration, except as stated in the Acknowledgements and specified in the text.

It is not substantially the same as any that I have submitted, or, is being concurrently submitted for a degree or diploma or other qualification at the University of Cambridge or at any other University or similar institution.

No substantial part of my dissertation has already been submitted, or, is being concurrently submitted for a degree or diploma or other qualification at the University of Cambridge or at any other University or similar institution.

Acknowledgements

This project was very much a team effort and I would first like to thank all the members of the integration project team. Thanks to David Ellis for designing and fabricating the devices, the devices were fabricated at the Cavendish and the e-beam lithography was undertaken by Jonathan Griffiths. Thanks to Thomas Meany for packaging the hybrid device and taking measurements, Frederick Floether for designing the devices, Jamie Lee for assisting with measurements and to Anthony Bennet for designing and taking measurements. Thanks also for Ian Farrer and the staff at the Cavendish for growing wafers. Thanks to Andrew Shields and David Ritchie for giving me this opportunity to study for this degree. This project was supported by the Initial Training Network PICQUE under the European Commission Marie Curie Actions.

Abstract

Fundamental to the future of quantum photonics is the ability to create integrated devices. An integrated chip offers intrinsic stability and compactness. This makes it inherently more scalable than a bulk optics approach. Quantum dots (QDs) are a developing on-chip source of single photons. This project aims to take quantum dots embedded in a III-V material and combine them with integrated waveguide components. The InAs QDs are grown in GaAs substrate and are bonded to a SiON based waveguide platform. This approach has potential for the realization of an efficient coupling between the quantum dots and the waveguides and then on-chip manipulation of the emitted photons. In this report, the results thus far will be presented and proposals for future designs will be discussed.

Publications resulting from this work

Quantum photonics hybrid integration platform

E. Murray, D. J. P. Ellis, T. Meany, F. F. Floether, J. P. Lee, J. P. Griffiths, G. A. C. Jones, I. Farrer, D. A. Ritchie, A. J. Bennett, and A. J. Shields.

Applied Physics Letters 107.17 (2015): 171108.

Editor's choice 2-8th November 2015

Cavity-enhanced coherent light scattering from a quantum dot A. J. Bennett, J. P. Lee, D. J. P. Ellis, T. Meany, **E. Murray**, F. F. Floether, J. P. Griffiths, I. Farrer, D. A. Ritchie, and A. J. Shields.

arXiv pre-print: 1508.01637v1

An all-electric scalable and tuneable single-photon source E. Murray & J. P. Lee, A. J. Bennett, J. Skiba-Szymanska, D. J. P. Ellis, I. Farrer, D. A. Ritchie, and A. J. Shields.

In-preparation

Conferences

Quantum dots for quantum information science,

E. Murray

PICQUE Integrated Quantum Photonics Workshop, 7-9 January 2015, Oxford, UK

Quantum photonics hybrid integration platform

E. Murray, D. J. P. Ellis, T. Meany, F. F. Floether, J. P. Lee, J. P. Griffiths, G. A. C. Jones, I. Farrer, D. A. Ritchie, A. J. Bennett, and A. J. Shields.

Best talk awarded PICQUE Roma Scientific School, 6-10 July 2015, Rome, Italy

Contents

Chapter 1

Results

Various approaches for embedding QDs into integrated circuits are being explored. Photonic crystal waveguides yield high coupling efficiency of the QD emission into the in-plane propagating waveguide mode [**?**]. They have also demonstrated in-plane indistinguishable photons [**?**]. QDs integrated with ridge waveguides in GaAs have been reported integrated with on-chip superconducting single photon detectors [**?**]. Air clad GaAs ridge waveguides have also demonstrated QD integrated directional couplers [**?**, **?**]. Other approaches use heralded single photons from spontaneous parametric down conversion integrated with waveguide chips [**?**] however this approach lacks the deterministic emission of quantum dots.

In this chapter, a platform for hybrid integration of III-V QDs with silicon oxynitride waveguides is presented. A GaAs chip containing InAs quantum dots are bonded orthogonally to the SiON chip such that the photons emitted from the surface of the GaAs chip are routed into a guided mode. The quantum dots are embedded in a low quality factor distributed Bragg reflector cavity with alternating layers of AlAs and GaAs. The SiON chip consists of a waveguide to deliver laser excitation light to the quantum dots and a return line through a Mach Zehnder interferometer. The orthogonal bonding method allows the surface emission from the QD to be collected by the waveguide. This orthogonal bonding is a major advantage of this hybrid integration method. The surface emission from the QD can be easily optimised by growing a distributed Bragg reflector cavity and/or creating a micropillar structure. Previous reports show efficiencies of out of plane

QD collection as high as 0.75 into free space high numerical aperture objectives [**?**, **?**]. In the device presented here, the SiON waveguide numerical aperture is 0.3. The hybrid platform also has the potential for diode structures to be created for electrically driven or tuneable QD devices integrated with the waveguides.

In this chapter, first theoretical simulations of the device are discussed. These calculations were used to deduce the theoretical efficiency of the device and to optimise parameters. Then the development of high-quality waveguides circuits is presented. Followed by a discussion of the created hybrid device. Sections of this chapter, specifically the Hybrid integrated devices section, are as a result of work which has been recently published [**?**].

1.1 Simulations and design

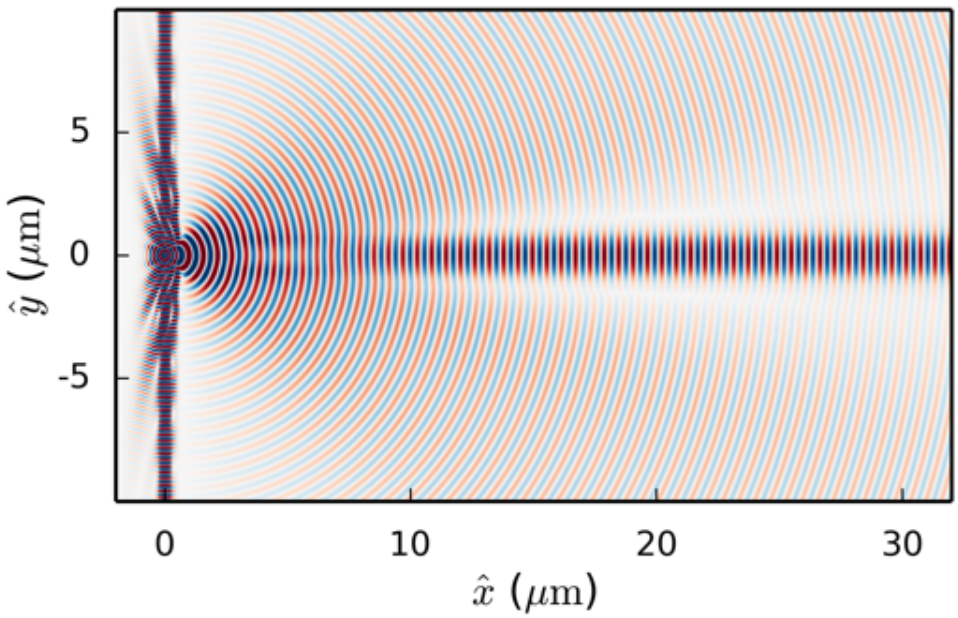

Figure 1.1: Finite difference time domain simulation of a QD dipole emitting in a cavity and the emission being guided by the SiON core.

The characteristics of the device were simulated by using the finite difference time domain package MEEP [**?**, **?**]. A $\hat{z}$ oriented dipole emitter was placed in the centre of the cavity spacer aligned to the

centre of the waveguide. A perfectly matched layer was placed at the edges of the simulation domain to absorb all light and prevent unwanted reflections. The $\hat{z}$ component of the electric field is shown in Figure 1.1. There is a clear emission pattern along the waveguide core. The efficiency of this device was also determined theoretically. A bounding box which records the Fourier transformed fields was placed at the edge of the domain and just inside the perfectly matched layer.

From this bounding box the total power spectrum is recorded when the system is excited with a short Gaussian pulse. Another flux plane is placed across the waveguide. The waveguide core size was 1.6 μm, in order to keep te guides single mode, and the far field propagating mode has a spatial $1/e$ width of 1.88 μm which was chosen as the size of the waveguide flux plane. It is placed sufficiently far from the surface of the III-V cavity enhanced-chip so that only the waveguide propagating mode is measured. Taking the ratio of the light propagating in the waveguide to the total in the bounding box gives the efficiency of the hybrid collection system. At the centre of the cavity wavelength the efficiency is 2.8%. For a QD emitting into free space with no cavity a collection of 0.5% can be expected into a 0.5 NA objective. When the QD is in a cavity the efficiency can rise to 7% depending on the number of mirror repeats and the numerical aperture of the collection objective. For the device presented here the numerical aperture of the waveguide is 0.35 and the III-V sample has a planar cavity with Bragg 12 repeats below the QD layer and 2 repeats above. This efficiency of 2.8% is almost exactly in line with what has previously been estimated for free space collection with the same NA and same number of repeats [**?**].

1.2 Waveguide devices

As explained in the Chapter 2, by placing two waveguides in close proximity the light can couple between them. The power in each waveguide at a position L is given by

$$P_1(L) = I\cos^2 cL \tag{1.1}$$

$$P_2(L) = I\sin^2 cL \tag{1.2}$$

where I is the input laser intensity, c is the coupling coefficient related to the waveguide index

contrast, the separation between the guides and the wavelength. These equations allow the design of DCs with a well defined coupling ratio by changing the interaction length L. To test this a set of chips were fabricated with DCs of increasing interaction length L and the coupling ration was measured for each. The results are shown in Figure 1.2. The differing black and red squares and circles are simply different chips from the same wafer. The red line is a $\sin^2$ fit to the data. The results show good consistency between chips, and the behaviour matches the expected sinusoid. This allows the creation of devices with embedded DCs with any coupling ratio, defined by the fabrication process. For example, to do on-chip Hanbury Brown and Twiss a DC with $r = 1/2$ is needed. For a photonic quantum CNOT gate a series of DCs with ratios $r = 1/2$ and $r = 1/3$ is needed.

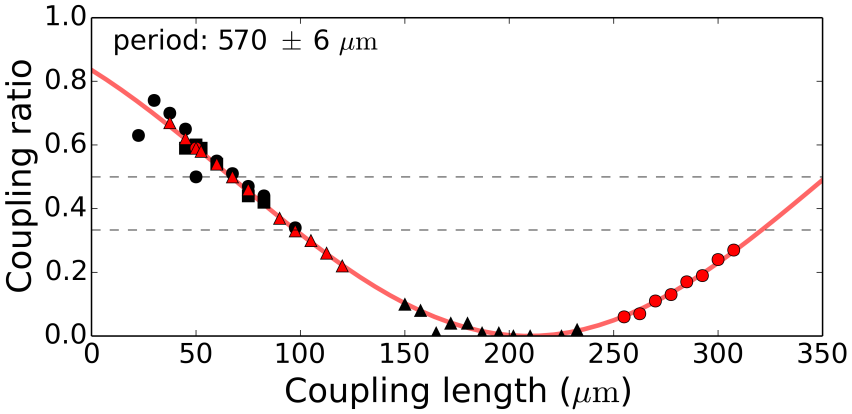

Figure 1.2: Measured coupling ratio vs interaction length for a set of waveguide chips. The results show the expected smooth sinusoidal behaviour.

Another important parameter for a waveguide device is its operating wavelength, depending on the III-V source used, the waveguide device would need to operate in the range 900-950nm for the current QD devices, however the QDs can achieve telecom wavelengths. The properties of a DC will change depending on the wavelength of the light. To check this, one DC was analysed by varying laser wavelength and monitoring the coupling ratio, this result is shown in Figure 1.3.

As is seen in Figure 1.3 , there is a linear decrease in the coupling ratio with increasing wavelength for the measured chip. In general the wavelength dependence is always linear, however whether the slope is positive or negative depends on other chip parameters, such as length, period of the length dependence and index contrast.

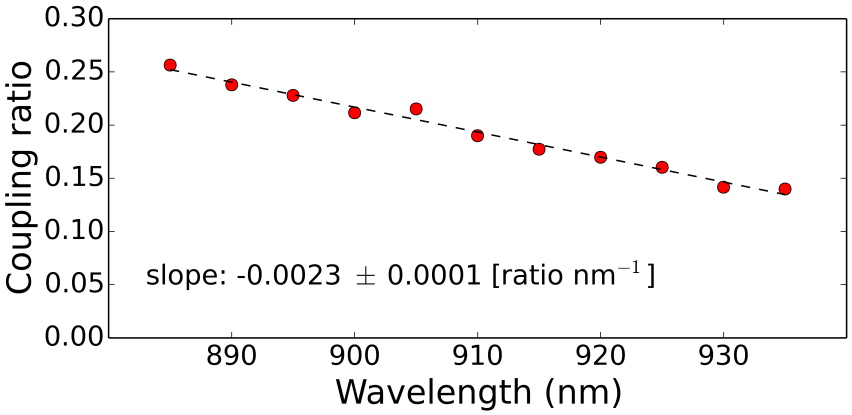

Figure 1.3: Measured DC coupling ration vs laser wavelength for a device. The red line is a linear fit to the data.

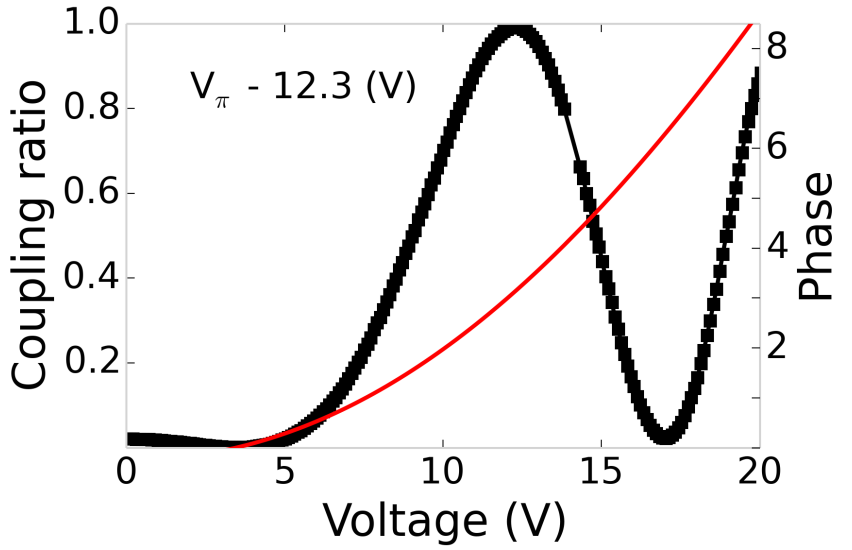

Figure 1.4: Performance of an SiON based Mach Zehnder interferometer. The black line traces the coupling ratio vs applied voltage and the red line is the phase calculated from the data.

Mach Zehnder interferometers are very interesting devices for their applications in quantum computing, by way of a qubit preparation device, and in telecommunications, as a light modulator. The MZIs were fabricated as described in Chapter 2 by placing two DCs in series with a phase changing element on one arm, in this case a heater causes a refractive index change which induces a phase change. The coupling ratio was monitored as the heater voltage was varied. The result is

shown in Figure 1.4. The black squares are the coupling ratio as the voltage was varied and the red line is the calculated phase. The phase was calculated using a pre-established model [**?**]. The visibility of this MZI was 99.7 ± 0.06 %. To apply a π phase shift to the light in one arm in this case would need 12.3 V applied to the heater.

In this section the development of high quality photonic circuits was described. Performing quantum operations on chip offers greater stability and scalability than can be done with bulk optics. In the next section the photonic circuits will be combined with the QD source in order to make an integrated platform capable of operating on the quantum light emitted by the QDs.

1.3 Hybrid integrated devices

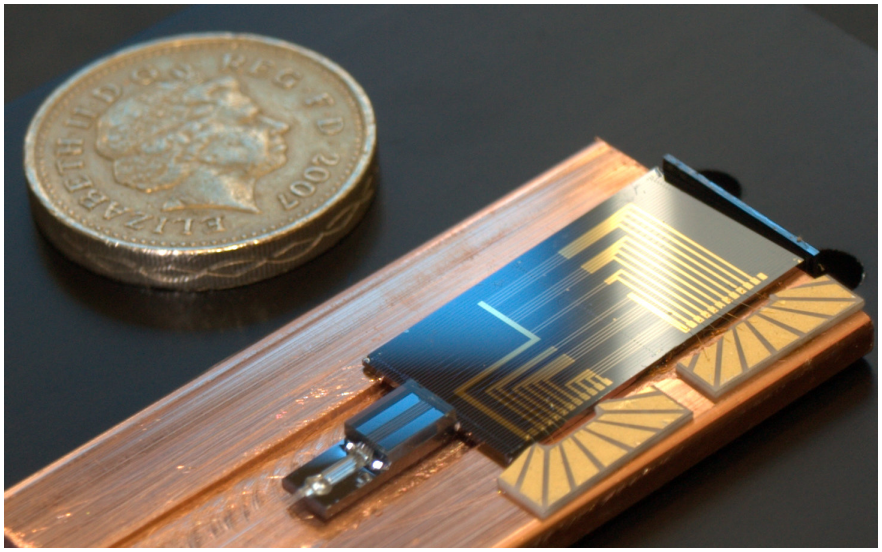

Figure 1.5: Photograph of an example bonded device.

Figure 1.5 shows a photograph of an example device. A strip of microcavity wafer containing QDs is bonded to one end of the SiON waveguide chip. In SiON the waveguide numerical aperture is limited by $\sqrt{n_{core}^2 - n_{clad}^2}$, where $n_{core} = 1.55$ and $n_{clad} = 1.51$. The photons are routed into the waveguides, two sequential directional couplers form a MZI with a nichrome heater applying a local phase shift to one MZI arm. This SiON technology is compatible with the creation of arbitrary designs of beamsplitters, MZIs and phase shifters. As explained in the previous chapter,

a polarisation maintaining fibre array is aligned and attached to the waveguides for collection of photons and the device is cooled to 4K for the duration of the experiment.

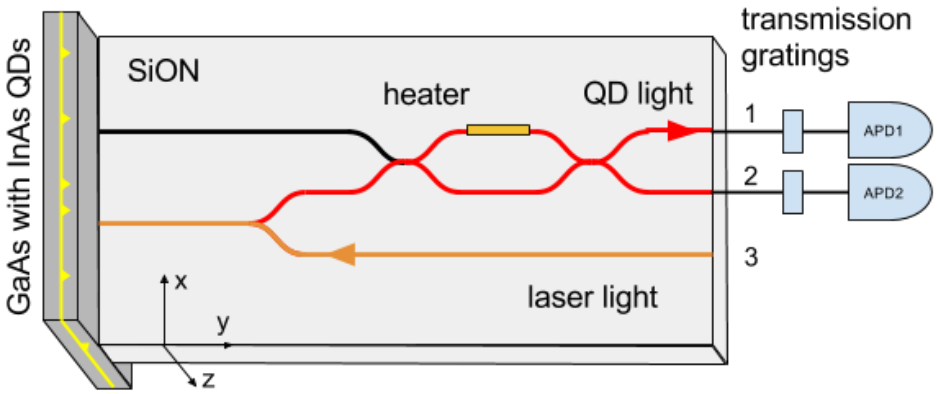

Figure 1.6: Schematic of the experiment.

Figure 1.6 shows the optical schematic of the experiments. A single channel delivers laser light. The QD light is returned through the MZI and collected into the fibre array. The fibres are sent directly to a spectrometer. For time resolved experiments transmission gratings are used to spectrally filter the emission before sending the light to avalanche photodiodes.

The integrated device is fixed and there is no freedom to analyse different QDs on the III-V sample once the bonding is complete. This creates stability and no drifting in emission intensity is seen over the course of 12 hours. The QD intensity as a function of time is plotted in Figure 1.9. A reasonably high density QD sample is used to ensure that a dot which is emits in the centre cavity mode is aligned with a waveguide. The central cavity wavelength is at 910nm. The spectrum from both outputs of the device can be seen in Figure 1.7. The MZI was tuned to 50:50, and it is seen that the spectrum from both output arms is identical. The QD analysed was the one at the centre of the cavity mode at 1.362 eV.

A power dependence was recorded, seen in Figure 1.8. The emission, before saturation, is approximately linear ($P^{0.95}$) implying an exciton and not a higher order complex [**?**]. The peak exhibits no fine structure splitting typically seen in a neutral exciton [**?**, **?**] so it is likely charged.

To verify the single photon nature of the QD emission, a Hanbury Brown and Twiss experiment was recorded using the on-chip MZI as a beamsplitter. The emission from both arms was sent through

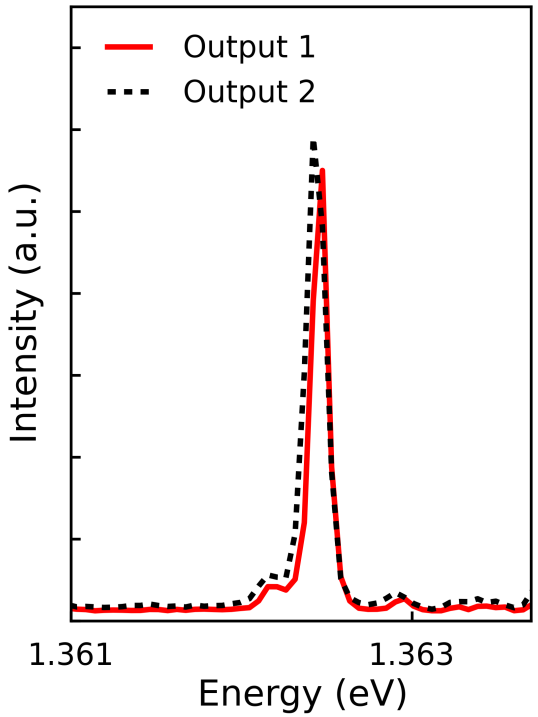

Figure 1.7: Spectrum of a quantum dot from both output ports of the device indicated in black and red.

two different transmission gratings for spectral filtering and then sent to avalanche photodiodes. The signal in one arm was delayed so as to measure negative correlation times. An absence of correlation coincidences at time $\tau = 0$ implies single photon emission. The second order correlation curves were taken under continuous wave (λ = 810nm) and pulsed (λ = 850nm) excitation. The curves are shown in Figure 1.10. In the case of the pulsed curve (shown in Figure 1.10 (a)) the signal to noise ratio due to dark counts, ($\sim$ 100 vs $\sim$ 1500 QD counts), of the detectors was calculated and the resulting dark count contribution was subtracted. A time window was also applied to the data. Since the lifetime of the QD was 670 $\pm$ 3ps, the vast majority (96%) of QD emission resides in a 4ns window. So only coincidences inside this window were used for calculating the $g^{(2)}(0)$ value of 0.19.

In the CW case as seen in Figure 1.10 (b) the black line corresponds to the data, the red solid line corresponds to a fit and the blue line to a deconvoluted fit. The deconvolution was done to subtract the response function of the detectors and timing system. The $g^{(2)}(0)$ was taken from the

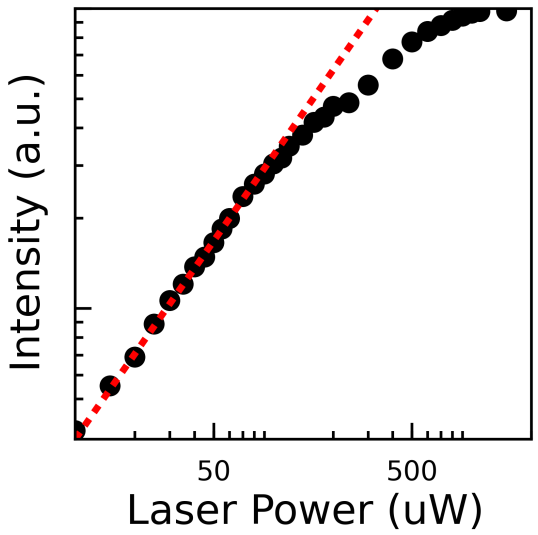

Figure 1.8: Recorded dependence of the QD emission intensity on the laser power, the solid line is a fit to the data. There is a linear dependance between QD intensity and laser power implying the transition is from an exciton state.

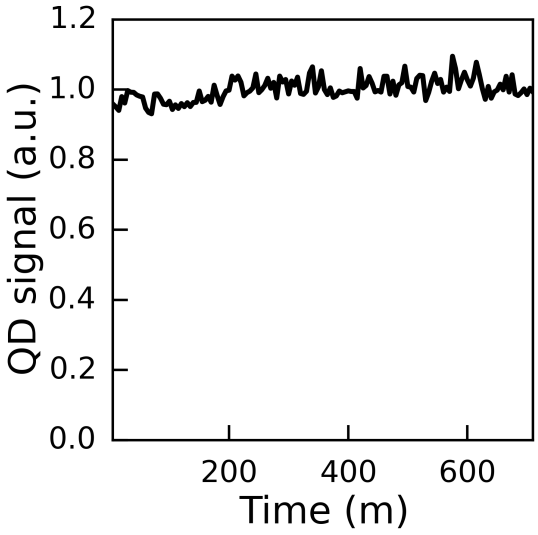

Figure 1.9: Counts measured as a function of time over 12 hours.

deconvoluted to be 0.09.

The active modulation of the MZI was tested on the single photon source. A voltage was applied to the heater on one arm of the MZI which induces local heating of the arm and a change in the

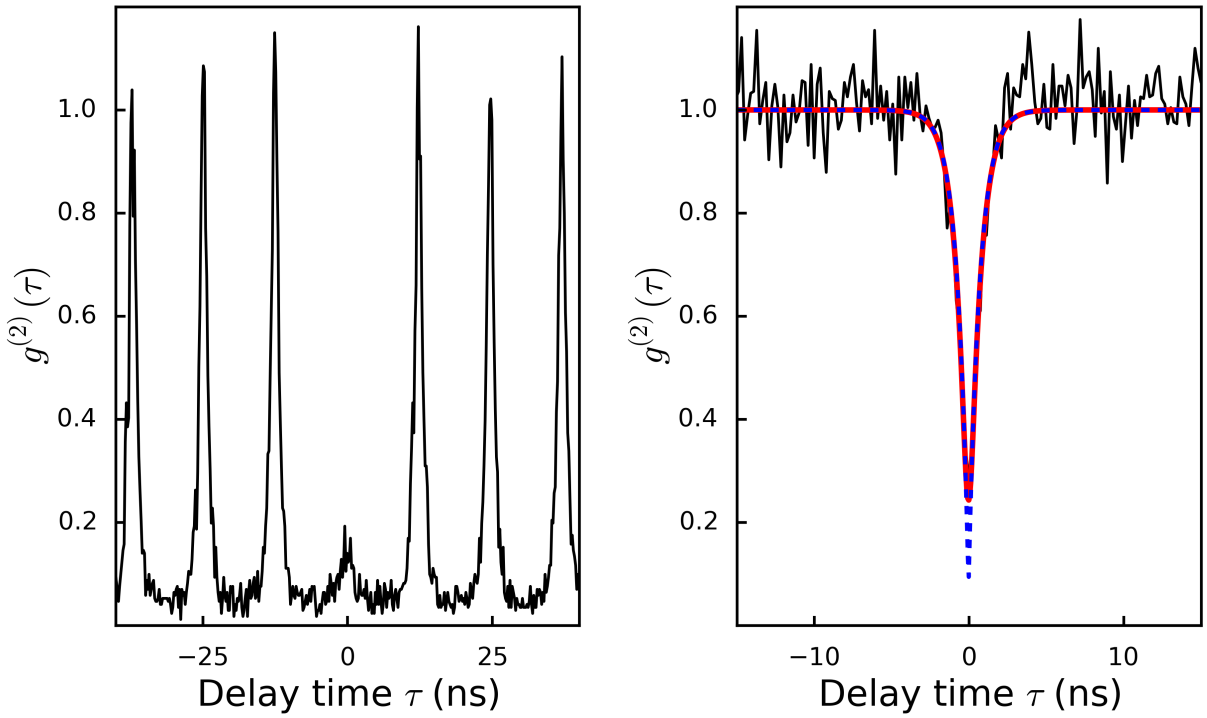

Figure 1.10: (a) Second order correlation function under pulsed excitation (b) Second order correlation function under continuous wave excitation. The black line is the raw data, the red line is a fit taking the system response function into account, and the dashed blue line is the fit deconvoluted with the response function.

refractive index of the waveguide core. This creates a relative phase between the light in each arm. The emission coupling to each output arm of the MZI then varies as a function of the applied voltage. This coupling, along with calculated phase, is shown in Figure 1.11.

The model was based on calculating the expected power output of each port as a function of coupling ratio and phase. The expected power is based on the matrix model of a phase shift operation between two directional couplers [**?**]. The model of the phase the same as the one used in Section 1.2[**?**].

In conclusion a novel method for integrating a III-V quantum light source with an SiON waveguide platform has been demonstrated. The single photon nature of the source was verified using on-chip components and the active modulation of the emission was demonstrated. This device shows

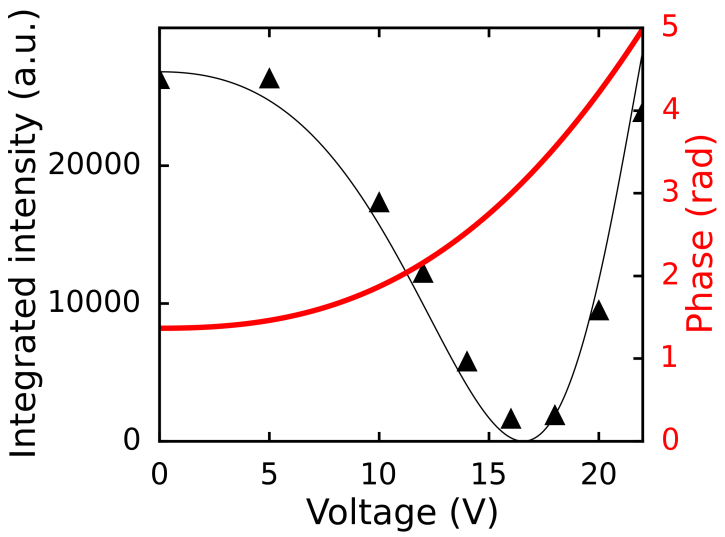

Figure 1.11: The outputs a MZI arm is shown by the black triangles, the solid black line is a fit to the data. The red line is the calculated phase as a function of voltage.

potential for integration of site controlled [**?**] QDs granting precise alignment of multiple QDs with multiple waveguides allowing for scalable quantum manipulation.

Bibliography

[1] Andre Schwagmann, Sokratis Kalliakos, Ian Farrer, Jonathan P Griffiths, Geb AC Jones, David A Ritchie, and Andrew J Shields. On-chip single photon emission from an integrated semiconductor quantum dot into a photonic crystal waveguide. *Applied Physics Letters*, 99(26):261108, 2011.

[2] Sokratis Kalliakos, Yarden Brody, Andre Schwagmann, Anthony J Bennett, Martin B Ward, David JP Ellis, Joanna Skiba-Szymanska, Ian Farrer, Jonathan P Griffiths, Geb AC Jones, et al. In-plane emission of indistinguishable photons generated by an integrated quantum emitter. *Applied Physics Letters*, 104(22):221109, 2014.

[3] Günther Reithmaier, Stefan Lichtmannecker, Thorsten Reichert, Peter Hasch, Kai Müller, Max Bichler, Rudolf Gross, and Jonathan J Finley. On-chip time resolved detection of quantum dot emission using integrated superconducting single photon detectors. *Scientific reports*, 3, 2013.

[4] N Prtljaga, RJ Coles, J O'Hara, B Royall, E Clarke, AM Fox, and MS Skolnick. Monolithic integration of a quantum emitter with a compact on-chip beam-splitter. *Applied Physics Letters*, 104(23):231107, 2014.

[5] Klaus D Jöns, Ulrich Rengstl, Markus Oster, Fabian Hargart, Matthias Heldmaier, Samir Bounouar, Sven M Ulrich, Michael Jetter, and Peter Michler. Monolithic on-chip integration of semiconductor waveguides, beamsplitters and single-photon sources. *arXiv preprint arXiv:1403.7174*, 2014.

[6] Thomas Meany, Lutfi A Ngah, Matthew J Collins, Alex S Clark, Robert J Williams, Benjamin J Eggleton, MJ Steel, Michael J Withford, Olivier Alibart, and Sébastien Tanzilli.

Hybrid photonic circuit for multiplexed heralded single photons. *Laser & Photonics Reviews*, 8(3):L42–L46, 2014.

[7] Julien Claudon, Joël Bleuse, Nitin Singh Malik, Maela Bazin, Périne Jaffrennou, Niels Gregersen, Christophe Sauvan, Philippe Lalanne, and Jean-Michel Gérard. A highly efficient single-photon source based on a quantum dot in a photonic nanowire. *Nature Photonics*, 4(3):174–177, 2010.

[8] Mathieu Munsch, Nitin S Malik, Emmanuel Dupuy, Adrien Delga, Joël Bleuse, Jean-Michel Gérard, Julien Claudon, Niels Gregersen, and Jesper Mørk. Dielectric gaas antenna ensuring an efficient broadband coupling between an inas quantum dot and a gaussian optical beam. *Physical review letters*, 110(17):177402, 2013.

[9] E. Murray, D. J. P. Ellis, T. Meany, F. F. Floether, J. P. Lee, J. P. Griffiths, G. A. C. Jones, I. Farrer, D. A. Ritchie, A. J. Bennett, and A. J. Shields. Quantum photonics hybrid integration platform. *Applied Physics Letters*, 107(17), 2015.

[10] Ardavan F Oskooi, David Roundy, Mihai Ibanescu, Peter Bermel, John D Joannopoulos, and Steven G Johnson. Meep: A flexible free-software package for electromagnetic simulations by the fdtd method. *Computer Physics Communications*, 181(3):687–702, 2010.

[11] Vladimir A Mandelshtam and Howard S Taylor. Harmonic inversion of time signals and its applications. *The Journal of chemical physics*, 107(17):6756–6769, 1997.

[12] AJ Bennett, P Atkinson, P See, MB Ward, RM Stevenson, ZL Yuan, DC Unitt, DJP Ellis, K Cooper, DA Ritchie, et al. Single-photon-emitting diodes: a review. *physica status solidi (b)*, 243(14):3730–3740, 2006.

[13] Jonathan CF Matthews, Alberto Politi, André Stefanov, and Jeremy L O'Brien. Manipulation of multiphoton entanglement in waveguide quantum circuits. *Nature Photonics*, 3(6):346–350, 2009.

[14] M Grundmann and D Bimberg. Theory of random population for quantum dots. *Physical Review B*, 55(15):9740, 1997.

[15] M Bayer, G Ortner, O Stern, A Kuther, AA Gorbunov, A Forchel, Pawel Hawrylak, S Fafard, K Hinzer, TL Reinecke, et al. Fine structure of neutral and charged excitons in self-assembled in (ga) as/(al) gaas quantum dots. *Physical Review B*, 65(19):195315, 2002.

[16] D Gammon, ES Snow, BV Shanabrook, DS Katzer, and D Park. Fine structure splitting in the optical spectra of single gaas quantum dots. *Physical review letters*, 76(16):3005, 1996.

[17] R Clark Jones. A new calculus for the treatment of optical systems. *JOSA*, 31(7):488–493, 1941.

[18] Gediminas Juska, Valeria Dimastrodonato, Lorenzo O Mereni, Agnieszka Gocalinska, and Emanuele Pelucchi. Towards quantum-dot arrays of entangled photon emitters. *Nature Photonics*, 7(7):527–531, 2013.